International Global Navigation Satellite Systems Association
IGNSS Conference 2016

Colombo Theatres, Kensington Campus, UNSW Australia
6 – 8 December 2016

Triple Frequency precise point positioning with multi-constellation GNSS

Manoj Deo
PhD Candidate, Department of Spatial Sciences, Curtin University,
GPO Box U 1987, Perth WA 6845, Australia
Phone: +61 432163000
Email: manoj.deo01@gmail.com

Ahmed El-Mowafy
Assoc. Professor, Department of Spatial Sciences, Curtin University,
GPO Box U 1987, Perth WA 6845, Australia
Phone: +61 8 9266 3403
Fax: +61 8 9266 2703
Email: a.el-mowafy@curtin.edu.au

ABSTRACT

The availability of signals on three or more frequencies from multiple GNSS constellations provides opportunities for improving precise point positioning (PPP) convergence time and accuracy, compared to when using dual-frequency observations from a single constellation. Although the multi-frequency and multi-constellation (MFMC) data may be used with present day precise orbit and clock products, there are several biases that must be considered to get the best results. When using IGS products, the precise orbit and clock corrections are generated using dual-frequency ionosphere-free combinations of a 'base' pair of signals, and usage of other signals in the PPP model results in differential code biases (DCB). Other biases to consider include differential phase biases (DPB) for the satellites and receiver and satellite antenna offsets for individual frequencies. Integrating multi-constellation data introduces additional biases, such as inter-system hardware and time biases and inter-frequency bias. Although the integration of MFMC data introduces such biases, it improves the measurement model strength and hence can potentially improve PPP performance through reducing solution convergence time and increasing precision and accuracy.
A brief overview of the MFMC biases and strategies that may be used to treat them is discussed. A proposed PPP model that uses triple frequency ionosphere-free low-noise linear combination for float ambiguity estimation is tested and analysed. MFMC data from four Australian sites is used to demonstrate the improvements in PPP solution convergence time, accuracy and precision, when comparing single- to multi-constellation GNSS data.

KEYWORDS: precise point positioning, multi-constellation, multi-frequency, biases, solution convergence.

1. INTRODUCTION

The PPP technique can determine the position of a GNSS receiver to cm-level accuracy for static surveying and sub-decimetre accuracy for kinematic applications, without relying on data from a single or network of reference stations. The first advent in PPP was made in Zumberge et al. (1997), where it was shown that cm-level repeatability can be achieved with dual-frequency undifferenced GPS measurements augmented with precise orbit and clock corrections. This is often known as the traditional PPP model, where the functional model consists of ionosphere-free linear combinations of dual-frequency pseudorange and carrier phase measurements. A major limitation of this technique is the time needed to achieve convergence of the solution to sub-decimetre accuracy, typically around 30 minutes, which restricts many real-time users from using this technique. At present, several commercial satellite subscription services provide real-time orbit and clock corrections for PPP such as StarFire (Deere), RTX (Trimble), Atlas (Hemisphere), Terrastar (Veripos) and MagicGNSS. However, convergence time remains to be a problem especially in areas obstructed by trees, buildings or canyons, where the PPP convergence is interrupted several times and for each time, the user needs to wait for the convergence to reoccur (Gakstter, 2016).

The availability of data on three or more frequencies from multiple GNSS constellations provides an opportunity for improving the PPP performance in terms of reducing the solution convergence time and increasing the accuracy and precision. However, such integration of MFMC data results in several biases and handling of these biases is a complex problem that requires careful modelling. We restrict attention here to the use of IGS precise orbit and clock corrections which are generated from ionosphere-free combinations of a 'base' pair of signals, (e.g. GPS L1/L2, Galileo E1/E5a and Beidou B1/B2) and usage of other signals in the PPP model results in differential code biases (DCB) which must be treated. Integration of MFMC data also results in other biases such as differential phase biases (DPB) (including the initial fractional phase biases) in the satellites and receiver, and satellite antenna offsets for individual frequencies (rather than the ionosphere-free combination of the 'base signal pair'), inter-system hardware and time biases (ISB and ISTB) and inter-frequency bias. A detailed analysis of these biases and recommendations for their modelling is presented in El-Mowafy et al. (2016).

The availability of triple frequency data may potentially reduce PPP convergence time, compared to the dual-frequency case. This will make the PPP technique more practical for real-time applications. Deo and El-Mowafy (2016a) compared the performance of three PPP models that use triple frequency data. However, the testing was done for a GPS only case. PPP with multi-constellation GNSS has been widely studied for dual-frequency measurements. Multi-constellation provides improved satellite geometry for better PPP performance in challenging environments like open-pit mines, urban canyons and forests. An early GPS-GLONASS combined PPP model was presented in Cai and Gao (2007), which showed improvements in accuracy and solution convergence time. A GPS-Galileo combined PPP model was attempted in Cao et al. (2010). Li et al. (2013) presented PPP results using GPS and Beidou integration, which had 12 satellites from the latter system at the time of writing. The results showed a slight improvement in convergence time, but only marginal improvement was noted in positioning accuracy. The traditional dual-frequency PPP model was adopted in all these studies, though

results were not conclusive due to the partial completion of the GLONASS, Galileo and Beidou constellations at the time of study..

In this paper, the PPP model that uses triple frequency ionosphere-free low-noise linear combination presented in Deo and El-Mowafy (2016a) is extended to a multi-constellation applications using GPS, Galileo and Beidou observations. This linear combination was developed for triple frequency data by applying three conditions of noise minimisation, ionosphere-free and geometry preservation. Firstly, the models for the MFMC observation equations are given, followed by a discussion of the biases and recommended practices for treating them. The next section presents the functional model for the triple frequency PPP model when using the three constellations, followed by a description of the stochastic modelling of observations. Next, the analysis and testing of data at four Australian GNSS continuous operating stations is presented. Results comparing the convergence time, accuracy and precision for triple frequency PPP using GPS only, GPS+Galileo, GPS+Beidou and GPS+Galileo+Beidou are presented next, followed by conclusions.

2. GNSS OBSERVATION MODEL

The observation equation of the carrier phase and pseudorange code measurements for satellite o from one GNSS constellation such as GPS (denoted as G) on frequency i in length units can be formulated as follows:

$$P_i^{oG} = \rho^{oG} + c\left(dt_{\mathrm{G}} - dt^{oG} + d_{i_G} - d_i{}^{oG}\right) + T^{oG} + \mu_i I^{oG} + \varepsilon_{\mathrm{P}_i}^{oG} \quad (1)$$

$$\phi_i^{oG} = \rho^{oG} + c(dt_{\mathrm{G}} - dt^{oG}) + T^{oG} - \mu_i I^{oG} + \lambda_i\left(N_i^G + \delta_{i_G} - \delta_i{}^{oG}\right) + \varepsilon_{\phi_i}^{oG} \quad (2)$$

where P_i^{oG} is the code and ϕ_i^{oG} is the phase measurement, ρ^{oG} is the satellite-to-receiver geometric range, c is the speed of light in vacuum; dt_{G} and dt^{oG} are the receiver and satellite clock offsets; $d_{i_{\mathrm{G}}}$ and $d_i{}^{oG}$ are the receiver and satellite code hardware biases in time units, respectively; δ_{i_G} and $\delta_i{}^{oG}$ are the receiver and satellite phase biases in cycles, respectively; N_i^G is the integer carrier phase ambiguity; T^{oG} is the tropospheric delay, $\mu_i = \frac{f_1^2}{f_i^2}$ is the dispersive coefficient of the ionosphere, I^{oG} is the ionosphere error for the L1 reference frequency; ε_{Pi}^{oG} and $\varepsilon_{\phi_i}^{oG}$ comprises code and phase measurement combined noise and multipath, respectively.

For the Beidou constellation (denoted as C) with frequency j from satellite p, the equations for carrier phase and pseudorange code measurement for frequency j are (El-Mowafy et al., 2016):

$$P_j^{pC} = \rho^{pC} + c\left(dt_G - dt^{pC} + d_{j_C} - d_j{}^{pC}\right) + T^{pC} + \mu_j I^{pC} + ISTB_{G-C} + \varepsilon_{P_j}^{pC} \quad (3)$$

$$\phi_j^{pC} = \rho^{pC} + c(dt_G - dt^{pC}) + T^{pC} - \mu_j I^{pC} + ISTB_{G-C} + \lambda_j\left(N_j^{pC} + \delta_{j_G} - \delta_j{}^{pC}\right) + \varepsilon_{\phi_j}^{pC} \quad (4)$$

The terms are similar to the ones described for system G above. $ISTB_{G-C}$ is the inter-system time bias between systems G and C (i.e. GPS and Beidou), combined for the receiver and the satellite. Similar equation is derived for the Galileo constellation (denoted as E). When integrating data from multiple constellations, users have to consider the differences in coordinate frames, particularly when using broadcast orbits. When using the precise orbits from International GNSS Service (IGS) or its subordinate Multi-GNSS Experiment (M-GEX), the

orbits for all constellations are consistent with International Terrestrial Reference Frame (ITRF).

3. MODELLING OF BIASES

This section describes the modelling of biases that occur in a single constellation as well as biases that occur when integrating multi-constellation GNSS data.

3.1 Single Constellation Biases

Satellite and receiver hardware biases
Exists for both code and phase measurements and caused by several sources including digital delays in the signal generator, signal distortion, the processing filters, correlator differences handling signal modulation, firmware biases, bandwidth dissimilarities, in addition to the signal path through the antenna, splitter, cabling, and amplifier. Hardware biases tend to be stable and slowly changing with time. At the receiver end, it is the same for signals of the same frequency from the same constellation. Thus, the receiver hardware biases can be modelled out by the use of between satellite single differencing (BSSD) (El-Mowafy et al., 2016). At the satellite end, hardware biases are stable for hours and will be constant for a typical PPP session, however this may differ for each satellite.

Differential Code Bias (DCB)
The code hardware biases are different for each frequency. Hence when the ionosphere-free or other combination is formed between different frequencies, the impacts of these differences in hardware biases are transferred to the combination. For GPS, as an example, the precise orbit and clock products from IGS are formed from the dual-frequency ionosphere-free combination of L1/L2 and its DCB is included with transmitted clock corrections. Thus, DCBs won't affect PPP code observations when using this combination, but it will be present if using individual signals, or other linear combinations and in phase observations because the same satellite clock offset is used for both code and phase observations. The DCBs of the base frequency that appear in the phase observations is usually lumped with the float carrier-phase ambiguity term. A full mathematical treatment of DCBs for such cases is discussed in El-Mowafy et al. 2016. The satellite DCB products from the IGS multi-GNSS Experiment (M-GEX) are now available for multi-frequency combinations of several constellations (Montenbruck et al., 2014). Since hardware biases are the same for signals from the same frequency and constellation, receiver DCBs are eliminated by forming BSSD.

The mathematical models for the code measurements, considering DCBs produced from M-GEX when applying IGS clock corrections, are written below for GPS and Galileo using RINEX version 3 notations.

For GPS:

$$CIC^{oG} = \rho^{*oG} - c\left(DCB_{C1W-C1C} + \frac{f_2^2}{f_1^2-f_2^2}DCB_{C1W-C2W}\right) \quad (5)$$

$$CIW^{oG} = \rho^{*oG} - c\left(\frac{f_2^2}{f_1^2-f_2^2}DCB_{C1W-C2W}\right) \quad (6)$$

$$C2W^{oG} = \rho^{*oG} - c\left(\frac{f_1^2}{f_1^2-f_2^2}DCB_{C1W-C2W}\right) \quad (7)$$

$$C5Q^{oG} = \rho^{*oG} - c\left(DCB_{C1W-C5Q} + \frac{f_2^2}{f_1^2-f_2^2}DCB_{C1W-C2W}\right) \quad (8)$$

$$C5X^{oG} = \rho^{*oG} - c\left(DCB_{C1W-C5X} + \frac{f_2^2}{f_1^2 - f_2^2} DCB_{C1W-C2W}\right) \quad (9)$$

with $\rho^{*oG} = \rho^{oG} + c(dt_{\mathrm{G}} - dt^{oG}{}_{IGS}) + T^{oG} + \mu_i I^{oG} + \varepsilon_{P_i}^{oG}$. The primary code measurements used to generate the broadcast clock corrections are C1W (P1) and C2W (P2). Note that the C2X and C2S code measurements may be converted to C2W as $C2W_r^{oG} = C2S_r^{oG} + (DCB_{C2W-C2S})$, $C2W_r^{oG} = C2X_r^{oG} + (DCB_{C2W-C2x})$.

For Galileo, the primary code measurements used to generate the broadcast clock corrections are C1X (E1 B+C) and C5X (E5a I+Q) (Uhlemann et al., 2015, Prange et al., 2015). Note that since the Galileo $DCB_{C1X-C1X}$ is not currently available, C1C is assumed to be equivalent to C1X, thus $DCB_{C1X-C1X} = 0$. Similarly $DCB_{C5X-C5Q}$ and $DCB_{C1X-C7Q}$ are not available; thus it is assumed that C5X=C5Q and C7X=C7Q. The DCB corrections are applied as

$$CIC^{q_E} = \rho^{*q_E} - c\left(DCB_{C1X-C1C} + \frac{f_{E5a}^2}{f_{E1}^2 - f_{E5a}^2} DCB_{C1X-C5X}\right) \quad (10)$$

$$CIX^{q_E} = \rho^{*q_E} - c\left(\frac{f_{E5a}^2}{f_{E1}^2 - f_{E5a}^2} DCB_{C1X-C5X}\right) \quad (11)$$

$$C5X^{q_E} = \rho^{*q_E} - c\left(\frac{f_{E1}^2}{f_{E1}^2 - f_{E5a}^2} DCB_{C1X-C5X}\right) \quad (12)$$

$$C5Q^{q_E} = \rho^{*q_E} - c\left(DCB_{C5X-C5Q} + \frac{f_{E1}^2}{f_{E1}^2 - f_{E5a}^2} DCB_{C1X-C5X}\right) \quad (13)$$

$$C7X^{q_E} = \rho^{*q_E} - c\left(DCB_{C1X-C7X} + \frac{f_{E5a}^2}{f_{E1}^2 - f_{E5a}^2} DCB_{C1X-C5X}\right) \quad (14)$$

$$C7Q^{q_E} = \rho^{*q_E} - c\left(DCB_{C1X-C7Q} + \frac{f_{E5a}^2}{f_{E1}^2 - f_{E5a}^2} DCB_{C1X-C5X}\right) \quad (15)$$

The impact of DCBs corrections on code point positioning in the aviation context is discussed in Deo and El-Mowafy (2016b).

Initial Fractional Phase Bias (IFPB) and Differential Phase Biases (DPB)

Initial fractional phase cycle bias exists in the satellite and receiver and is always less than 1 phase cycle. It is separate from the hardware phase bias and constant for each session which is reset each time the receiver is switched off and on. IFPB is different for each frequency, but at the receiver end it is assumed the same for signals on the same frequency for satellites on the same constellation. Thus it is eliminated by forming BSSD measurements from the same frequency and constellation.

Differential Phase bias (DPB) also exists when forming linear combinations, due to the phase hardware biases being different for each frequency. BSSD measurements from the same frequency and constellation will eliminate DPB at the receiver end. However, the satellite DPB remains in the PPP model. Satellite DPBs are stable like the IFPB, but they are difficult to separate from each other. Therefore they are usually combined in one term, i.e. the DPB. In PPP with float ambiguity estimation, these are usually lumped with the non-integer carrier phase ambiguity term. For PPP-AR, the estimation of DPB is the key to enable integer ambiguity resolution.

3.2 Multi-constellation Biases

Inter-System Time Bias (ISTB)
The ISTB is due to each constellation having the satellite clocks referenced to the constellation own timescale. The ISTBs are accounted for by either estimating a separate bias for each system, or by estimating the bias for one system and then estimating the differences from other systems with reference to this system.

Inter System Biases (ISB)
As discussed earlier, the signals from different frequencies and constellations will have different hardware biases for code and phase observations (Hergarty et al, 2004). When a common receiver clock offset is used, which include biases of a primary system, for all constellations, the differences between the receiver biases for different constellations form the ISB. Thus, additional parameters must be introduced in the PPP model to account for these differences are known as inter-system biases (ISB).

4. TRIPLE FREQUENCY PPP MODEL

In this section, the functional and stochastic models for a triple frequency multi-constellation PPP method are described. The constellations included in the modelling include GPS (G), Beidou (C) and Galileo (E). It is assumed that the MFMC biases have been applied to the observations as discussed in El-Mowafy et al. (2016).

4.1 Functional Model

In the subsequent modelling, the ISTB is merged with the ISB term, the DPB and IFPB are merged with the float ambiguity term, whereas DCBs are applied to code measurements as described earlier using MGEX published DCB values. A low noise triple frequency ionosphere-free combination developed in Deo and El-Mowafy (2016a) is used as the observations in the functional model. This linear combination has least noise propagation properties, is first order ionosphere-free; and preserves geometry. It is applied separately for the multi-constellation code and phase observations, which have the same coefficients for each measurement. Due to the minimisation of code noise propagation, the PPP solution can converge faster than when using standard dual-frequency ionosphere-free combination. The actual noise reduction was 14% for GPS, 3.1% for Galileo and 1.1% for Beidou; whereas the convergence time reduced by 11% for tests done for GPS only data (Deo and El-Mowafy, 2016a). The equations for functional models for GPS, Beidou and Galileo are:

For GPS:

$$P^{o_G} = \alpha_{1,G} \cdot P_{L1}^{q_G} + \alpha_{2,G} \cdot P_{L2}^{o_G} + \alpha_{3,G} \cdot P_{L5}^{o_G} = \rho^{o_G} + cdt_{\mathrm{G}} + T^{o_G} + \varepsilon_{\mathrm{P}}^{o_G} \quad (16)$$

$$\phi^{o_G} = \alpha_{1,G} \cdot \phi_{L1}^{q_G} + \alpha_{2,G} \cdot \phi_{L2}^{o_G} + \alpha_{3,G} \cdot \phi_{L5}^{o_G} = \rho^{o_G} + cdt_{\mathrm{G}} + T^{o_G} + \lambda N^{*o_G} + \varepsilon_{\phi}^{o_G} \quad (17)$$

with the coefficient values being $\alpha_{1,G} = 2.326\,944$, $\alpha_{2,G} = -0.359\,646$, and $\alpha_{3,G} = -0.967\,299$

For Beidou:

$$P^{p_C} = \alpha_{1,C} \cdot P_{B1}^{p_C} + \alpha_{2,C} \cdot P_{B2}^{p_C} + \alpha_{3,C} \cdot P_{B3}^{p_C} = \rho^{p_C} + cdt_G + T^{p_C} + ISB_{G-C} + \varepsilon_{P_j}^{p_C} \quad (18)$$

$$\phi^{p_C} = \alpha_{1,C} \cdot \phi_{B1}^{p_C} + \alpha_{2,C} \cdot \phi_{B2}^{p_C} + \alpha_{3,C} \cdot \phi_{B3}^{p_C} = \rho^{p_C} + cdt_G + T^{p_C} + ISB_{G-C} + \lambda N^{*p_C} + \varepsilon_{\phi}^{p_C} \quad (19)$$

with the coefficient values being $\alpha_{1,C} = 2.566\,439$, $\alpha_{2,C} = -1.228\,930$, and $\alpha_{3,C} = -0.337\,510$

For Galileo:

$$P^{q_E} = \alpha_{1,E} \cdot P_{E1}^{q_E} + \alpha_{2,E} \cdot P_{E5a}^{q_E} + \alpha_{3,E} \cdot P_{E5b}^{q_E} = \rho^{q_E} + cdt_G + T^{q_E} + ISB_{G-E} + \varepsilon_P^{q_E} \quad (20)$$

$$\phi^{q_E} = \alpha_{1,E} \cdot \phi_{E1}^{q_E} + \alpha_{2,E} \cdot \phi_{E5a}^{q_E} + \alpha_{3,E} \cdot \phi_{E5b}^{q_E} = \rho^{q_E} + cdt_G + T^{q_E} + ISB_{G-C} + \lambda N^{*q_E} + \varepsilon_{\phi}^{q_E} \quad (21)$$

with coefficient values being $\alpha_{1,E} = 2.314\,925$, $\alpha_{2,E} = -0.836\,269$, and $\alpha_{3,E} = -0.478\,656$.

If we consider the case of a GNSS receiver tracking $1 \ldots n$ GPS satellites, $1 \ldots m$ Beidou satellites, and $1 \ldots k$ Galileo satellites at an instant of time. The unknown parameters are

$$\boldsymbol{x} = [x \quad y \quad z \quad cdt_G \quad ZWD \quad ISB_{G-C} \quad ISB_{G-E} \quad \lambda N^{*}(G1, \ldots, Gn, C1, \ldots, Cm, E1, \ldots, Ek)] \quad (22)$$

Where x, y, z denotes the unknown receiver position; ZWD is the zenith wet delay after modelling the hydrostatic tropospheric delay using the Saastamoinen model and expressing the wet delay as a function of a wet mapping function (Tuka and El-Mowafy, 2011). The ambiguity terms for each satellite are float values due to the presence of DPB of the considered signals and DCBs of the base frequencies. The functional model in Eqs. 16-21 is non-linear, and thus the system is linearised around approximate values of the unknown parameters, $\boldsymbol{x_0}$. Small corrections, $\Delta\boldsymbol{x}$, are calculated using Kalman filter, which is applied to the approximations to get the parameter estimates as $\boldsymbol{x} = \boldsymbol{x_0} + \Delta\boldsymbol{x}$. The design matrix, A, for this system is:

$$A = \begin{bmatrix}
\frac{X^{G1}-x_0}{\rho_0} & \frac{Y^{G1}-y_0}{\rho_0} & \frac{Z^{G1}-z_0}{\rho_0} & 1 & m_w & 0 & 0 & 0 & 0 & 0 & 0 & 0 & 0 & 0 \\
\frac{X^{G1}-x_0}{\rho_0} & \frac{Y^{G1}-y_0}{\rho_0} & \frac{Z^{G1}-z_0}{\rho_0} & 1 & m_w & 0 & 0 & 1 & 0 & 0 & 0 & 0 & 0 & 0 \\
\vdots & \vdots & \vdots & \vdots & \vdots & \vdots & \vdots & \vdots & \vdots & \vdots & \vdots & \vdots & \vdots & \vdots \\
\frac{X^{Gn}-x_0}{\rho_0} & \frac{Y^{Gn}-y_0}{\rho_0} & \frac{Z^{Gn}-z_0}{\rho_0} & 1 & m_w & 0 & 0 & 0 & 0 & 0 & 0 & 0 & 0 & 0 \\
\frac{X^{Gn}-x_0}{\rho_0} & \frac{Y^{Gn}-y_0}{\rho_0} & \frac{Z^{Gn}-z_0}{\rho_0} & 1 & m_w & 0 & 0 & 0 & 0 & 1 & 0 & 0 & 0 & 0 \\
\frac{X^{C1}-x_0}{\rho_0} & \frac{Y^{C1}-y_0}{\rho_0} & \frac{Z^{C1}-z_0}{\rho_0} & 1 & m_w & 1 & 0 & 0 & 0 & 0 & 0 & 0 & 0 & 0 \\
\frac{X^{C1}-x_0}{\rho_0} & \frac{Y^{C1}-y_0}{\rho_0} & \frac{Z^{C1}-z_0}{\rho_0} & 1 & m_w & 1 & 0 & 0 & 0 & 0 & 1 & 0 & 0 & 0 \\
\vdots & \vdots & \vdots & \vdots & \vdots & \vdots & \vdots & \vdots & \vdots & \vdots & \vdots & \vdots & \vdots & \vdots \\
\frac{X^{Cm}-x_0}{\rho_0} & \frac{Y^{Cm}-y_0}{\rho_0} & \frac{Z^{Cm}-z_0}{\rho_0} & 1 & m_w & 1 & 0 & 0 & 0 & 0 & 0 & 0 & 0 & 0 \\
\frac{X^{Cm}-x_0}{\rho_0} & \frac{Y^{Cm}-y_0}{\rho_0} & \frac{Z^{Cm}-z_0}{\rho_0} & 1 & m_w & 1 & 0 & 0 & 0 & 0 & 0 & 1 & 0 & 0 \\
\frac{X^{E1}-x_0}{\rho_0} & \frac{Y^{E1}-y_0}{\rho_0} & \frac{Z^{E1}-z_0}{\rho_0} & 1 & m_w & 0 & 1 & 0 & 0 & 0 & 0 & 0 & 0 & 0 \\
\frac{X^{E1}-x_0}{\rho_0} & \frac{Y^{E1}-y_0}{\rho_0} & \frac{Z^{E1}-z_0}{\rho_0} & 1 & m_w & 0 & 1 & 0 & 0 & 0 & 0 & 0 & 1 & 0 \\
\vdots & \vdots & \vdots & \vdots & \vdots & \vdots & \vdots & \vdots & \vdots & \vdots & \vdots & \vdots & \vdots & \vdots \\
\frac{X^{Ek}-x_0}{\rho_0} & \frac{Y^{Ek}-y_0}{\rho_0} & \frac{Z^{Ek}-z_0}{\rho_0} & 1 & m_w & 0 & 1 & 0 & 0 & 0 & 0 & 0 & 0 & 0 \\
\frac{X^{Ek}-x_0}{\rho_0} & \frac{Y^{Ek}-y_0}{\rho_0} & \frac{Z^{Ek}-z_0}{\rho_0} & 1 & m_w & 0 & 1 & 0 & 0 & 0 & 0 & 0 & 0 & 1
\end{bmatrix} \tag{23}$$

where m_w is the wet mapping function. The parameter matrix and the design matrix must be dynamically updated when new satellites appear, or when a satellite disappears from view. The initial values of the float ambiguities must be recalculated for a new satellite, when a satellite reappears after loss of tracking, or when a cycle slips is detected that cannot be repaired.

4.2 Stochastic Model of Observations

For stochastic modelling of GPS observations, which is equally applicable for Beidou and Galileo, the raw measurements are assumed to be uncorrelated with code noise $\sigma_{P_1^G}$, $\sigma_{P_2^G}$ and $\sigma_{P_5^G}$, and carrier phase noise $\sigma_{\phi_1^G}$, $\sigma_{\phi_2^G}$ and $\sigma_{\phi_5^G}$. Thus, the noise in the triple frequency code and phase linear combinations is determined with error propagation law as:

$$\sigma_{P^G}^2 = \left(\alpha_{1,G} \cdot \sigma_{P_1^G}\right)^2 + \left(\alpha_{2,G} \cdot \sigma_{P_2^G}\right)^2 + \left(\alpha_{3,G} \cdot \sigma_{P_5^G}\right)^2 \tag{24}$$

$$\sigma_{\phi^G}^2 = \left(\alpha_{1,G} \cdot \sigma_{\phi_1^G}\right)^2 + \left(\alpha_{2,G} \cdot \sigma_{\phi_2^G}\right)^2 + \left(\alpha_{3,G} \cdot \sigma_{\phi_5^G}\right)^2 \tag{25}$$

The measurement weighting is based on elevation angle (E) of the satellites as $1/\sin(E)$. Since the code and phase observations on different frequencies are assumed uncorrelated, the measurement covariance matrix is diagonal, where the linear combinations used in the model are also uncorrelated.

5. VALIDATION OF MULTI-CONSTELLATION PPP MODEL

5.1 Test Description

Test data was simulated for one day at four sites at Hobart (HOB2), Alice Springs (ALIC), Yarragadee (YAR2) and Townsville (TOW2), which are distributed over the Australian continent. Simulated data was used due to issues in actual data such as the line bias variations in GPS Block IIF satellites (Montenbruck et al., 2012), insufficient number of GPS Block IIF satellites, and the unavailability of satellite antenna phase centre offsets for individual signals. The GPS satellite antenna offsets are available for the L1-L2 ionosphere-free combination only, whereas the offsets for Galileo and Beidou are based on satellite design diagrams rather than actual calibrations. Dilssner et al. (2014) calibrated these offsets for Beidou satellites and reported that these were vastly different from the IGS M-GEX recommended values, by as much as 3.9m (for IGSO. Hence simulated data is used to isolate these issues and focus on the performance of the PPP model. The epoch interval rate was 30 s, with measurement standard deviations of 0.01 cycles for carrier phase on all frequencies, and for code measurements: 0.37m, 0.48m and 0.36m for GPS P1, P2 & P5; 0.36m, 0.35m and 0.34m for Galileo E1, E5a & E5b codes and 0.51m, 0.37m and 0.34m for Beidou B1, B2 & B3. These values are based on a method for determining the standard deviations presented in El-Mowafy (2014 and 2015) using a single-receiver single-channel method. A satellite elevation cut-off of 10 degrees was used.

5.2 Analysis and Discussion of Results

The triple frequency MFMC PPP model was implemented applying Kalman filter processing using by an in-house software. The software is suitable for processing kinematic data was configured for static data. The performance of the MFMC PPP model was assessed based on comparing the convergence time and positional accuracy to the standard dual-frequency solutions, after a 3 dimensional (3D) precision of 5cm was reached and maintained. Accuracy is defined as the root mean squared errors (RMSE) in East, North and up directions with respect to the known station position, after convergence is achieved.

- The mean RMSE and convergence times for the four sites when processing hourly blocks of data are given in Table 1. The algorithms compared are the standard dual-frequency GPS only solution (L1-L2 G) and the triple frequency solutions for GPS only, GPS+Beidou (G+C) and GPS+Beidou+Galileo (G+C+E). Overall, when comparing the triple frequency solutions to the conventional dual-frequency solution, the triple frequency solution for G+C+E gave the best performance with a notable improvement 7.6 minutes in convergence time and improvements of 2mm in RMSE East. More specifically at the four sites. For ALIC, the triple frequency solution for G+C gave the best performance with an improvement of 5mm in RMSE East and 5.7 minutes in convergence time.
- For HOB2, triple frequency solution for G+C+E gave the best performance with improvement of 4mm in RMSE up and 7.4 minutes in convergence time.
- For TOW2, triple frequency solution for G+C+E gave the best performance with improvement of 4mm in RMSE up and 7.7 minutes in convergence time.
- For YAR2, triple frequency solution for G+C+E gave the best performance with a notable improvement 11.5 minutes in convergence time. There was no noticeable improvement in accuracy, whereas the triple frequency solution for G had a slightly higher convergence time than the dual-frequency results.

Figure 1 shows, as an example, the PPP 3D positioning hourly solution errors at YAR2 for three triple frequency solutions using GPS only, GPS+Beidou and GPS+Beidou+Galileo as well as the conventional dual-frequency observations using GPS only observations. The improved performance of the MFMC PPP models, compared to the dual-frequency model is clearly visible with reduced convergence time and RMSE values.

Site	Solution	Mean RMSE East (m)	Mean RMSE North (m)	Mean RMSE Up (m)	Mean Convergence time (min)
ALIC	L1-L2 G	0.017	0.006	0.015	26.9
	Triple freq. G	0.018	0.006	0.014	24.9
	Triple freq. G+C	0.012	0.007	0.016	21.2
	Triple freq. G+C+E	0.012	0.007	0.018	22.1
HOB2	L1-L2 G	0.015	0.006	0.021	31.9
	Triple freq. G	0.012	0.007	0.017	25.8
	Triple freq. G+C	0.012	0.008	0.018	26.8
	Triple freq. G+C+E	0.014	0.007	0.017	24.5
TOW2	L1-L2 G	0.014	0.004	0.019	30.9
	Triple freq. G	0.012	0.005	0.015	26.3
	Triple freq. G+C	0.012	0.006	0.017	24.4
	Triple freq. G+C+E	0.014	0.007	0.015	23.2
YAR2	L1-L2 G	0.017	0.007	0.015	28.6
	Triple freq. G	0.016	0.006	0.019	30.0
	Triple freq. G+C	0.013	0.006	0.015	18.2
	Triple freq. G+C+E	0.017	0.005	0.015	17.1
Overall	L1-L2 G	0.016	0.006	0.018	29.6
	Triple freq. G	0.014	0.006	0.016	26.5
	Triple freq. G+C	0.012	0.007	0.016	23.0
	Triple freq. G+C+E	0.014	0.007	0.016	22.0

Table 1. Table of results showing mean RMSE and convergence times with hourly blocks of data for the conventional dual-frequency GPS only solution (L1-L2 G) and the triple frequency solutions for GPS only, GPS+Beidou (G+C) and GPS+Beidou+Galileo (G+C+E).

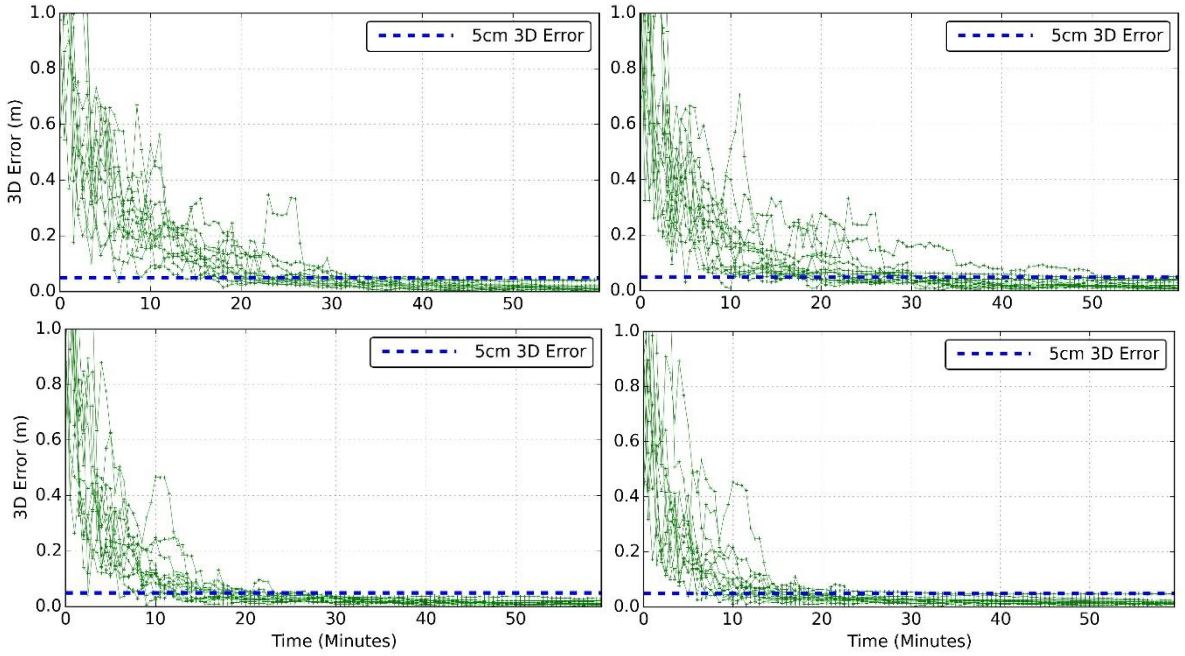

Figure 1. PPP 3-dimensional positioning errors for the hourly solutions at YAR2 for the standard dual-frequency GPS only solution (top-left) and the triple frequency solutions for GPS only (top-right), GPS+Beidou (bottom-left) and GPS+Beidou+Galileo (bottom-right).

6. CONCLUSIONS

An overview of the various biases that need to be considered when integrating MFMC data was given. A low-noise, ionosphere-free triple frequency PPP model proposed in Deo and El-Mowafy (2016a) was tested with hourly blocks of multi-constellation data from GPS, Beidou and Galileo at four sites covering the Australian continent. Improvements in both positioning accuracy by up to 5mm RMSE and convergence times by up to 11.5 minutes were noted at all four sites, when using the triple-frequency data compared to GPS-only dual-frequency PPP. Overall, the triple frequency solution for GPS+Beidou+Galileo gave the best performance with a notable overall improvement of 7.6 minutes in convergence time and improvements of 2mm in RMSE East and Up. This is a promising step for real-time PPP users who can potentially benefit from MFMC PPP.

REFERENCES

Cai C, Gao Y (2007) Precise Point Positioning Using Combined GPS and GLONASS Observations, *Journal of Global Positioning Systems*, 6(1): 13-22.

Cao W, Hauschild A, Steigenberger P, Langley RB, Urquhart L, Santos M and Montenbruck O (2010) Performance Evaluation of Integrated GPS/GIOVE Precise Point Positioning, *Proceedings of ITM 2009*, The Institute of Navigation International Technical Meeting, 25-27 January 2010, San Diego, California, pp. 540-552.

Deo MN, El-Mowafy (2016a) Triple Frequency GNSS Models for PPP with Float Ambiguity Estimation – Performance Comparison using GPS, *Survey Review*, published online 3 Dec 2016, http://dx.doi.org/10.1080/00396265.2016.1263179.

Deo MN, El-Mowafy (2016b) Evaluation of accuracy and availability of ARNS multi-constellation signals for aviation users in Australia, *IGNSS Conference 2016*, UNSW Australia, 6–8 December 2016.

Dilssner F, Springer T, Schönemann E, Enderle W (2014) Estimation of satellite antenna phase center corrections for BeiDou, *IGS Workshop*, Pasadena, California, USA (2014).

El-Mowafy A (2014). GNSS Multi-frequency Receiver Single-Satellite Measurement Validation Method, *GPS Solutions*, 18(4), 553-561.

El-Mowafy A (2015) Estimation of Multi-Constellation GNSS Observation Stochastic Properties Using a Single-Receiver Single-Satellite Data Validation Method, *Survey Review*, 47(341), 99-108.

El-Mowafy A, Deo M, Rizos C (2016) On biases in precise point positioning with multi-constellation and multi-frequency GNSS data, *Measurement Science and Technology*, 27 (2016), 10pp.

Gakstatter E (2016) ION GNSS+ a playground for high precision, *Geospatial Solutions*, September 22, 2016,< http://geospatial-solutions.com/ion-gnss-a-playground-for-high-precision-gnss/ >

Li W, Teunissen P, Zhang B and Verhagen S (2013) Precise Point Positioning Using GPS and Compass Observations, China Satellite Navigation Conference (CSNC) 2013 Proceedings, J. Sun et al. (eds.) , Springer-Verlag Berlin Heidelberg 2013.

Montenbruck O, Hauschild A and Steigenberger P (2014) Differential Code Bias Estimation using Multi-GNSS Observations and Global Ionosphere Maps, *Navigation*, 61(3): 191–201, Fall 2014.

Montenbruck O, Hugentobler U, Dach R, Steigenberger P, Hauschild A (2012) Apparent Clock Variations of the Block IIF-1 (SVN62) GPS Satellite, *GPS Solutions*, 16(3):303-313.

Prange L, Dach R, Lutz S, Schaer S, Jäggi A (2015) The CODE M-GEX Orbit and Clock Solution, *International Association of Geodesy Symposia*, Springer, Switzerland, 1-7.

Uhlemann M, Gendt G, Ramatschi M, Deng Z (2015) GFZ Global Multi-GNSS Network and Data Processing Results, *International Association of Geodesy Symposia*, Springer, Switzerland, 1-7.

Zumberge JF, Heflin MB, Jefferson DC, Watkins MM, Webb FH (1997) Precise Point Positioning for the Efficient and Robust Analysis of GPS Data from Large Networks, *Journal of Geophysical Research*, 102(B3): 5005-5017.